



HAL
open science

Changes in the atmospheric dynamics leading to West European summer hot temperatures since 1900

M Carmen Alvarez-Castro, Davide Faranda, Pascal Yiou

► **To cite this version:**

M Carmen Alvarez-Castro, Davide Faranda, Pascal Yiou. Changes in the atmospheric dynamics leading to West European summer hot temperatures since 1900. 2016. hal-01370975v1

HAL Id: hal-01370975

<https://hal.science/hal-01370975v1>

Preprint submitted on 23 Sep 2016 (v1), last revised 23 Nov 2017 (v3)

HAL is a multi-disciplinary open access archive for the deposit and dissemination of scientific research documents, whether they are published or not. The documents may come from teaching and research institutions in France or abroad, or from public or private research centers.

L'archive ouverte pluridisciplinaire **HAL**, est destinée au dépôt et à la diffusion de documents scientifiques de niveau recherche, publiés ou non, émanant des établissements d'enseignement et de recherche français ou étrangers, des laboratoires publics ou privés.

1 Changes in the atmospheric dynamics leading to 2 West European summer hot temperatures since 1900

M. Carmen Alvarez-Castro,¹ Davide Faranda,¹ and Pascal Yiou¹

3 Key points:

- 4 • Description of Western European heat events, in summer, that includes the dynamics of the
5 atmospheric circulation since 1871.
- 6 • The atmospheric circulation patterns leading summer heat events have changed during the
7 last century.
- 8 • Increasing trend of extreme hot summer temperatures associated to blocking episodes.

Corresponding author: M. Carmen Alvarez-Castro, LSCE. (carmen.alvarez-castro@lsce.ipsl.fr)

¹Laboratoire des Sciences du Climat et de
l'Environnement, UMR 8212
CEA-CNRS-UVSQ, IPSL, Université
Paris-Saclay, F-91191 Gif-sur-Yvette, France

9 **Abstract** Summer hot temperatures have many impacts on health, econ-
10 omy (agriculture, energy, transports) and ecosystems. In western Europe, the
11 recent summers of 2003 and 2015 were exceptionally warm. Many studies have
12 shown that the genesis of the major heat events of the last decades was linked
13 to anticyclonic atmospheric circulation and to spring precipitation deficit in
14 southern Europe. Such results were obtained for the second part of the 20th
15 century and projections into the 21st century. In this paper, we challenge this
16 vision by investigating the earlier part of the 20th century from an ensem-
17 ble of 20CR reanalyses. We propose an innovative description of Western-
18 European heat events that takes into account the dynamics of the circula-
19 tion. We argue that the atmospheric circulation patterns leading to the most
20 intense heat events have changed during the last century. We also show that
21 the increasing temperature trend during major heatwaves is encountered dur-
22 ing episodes of Scandinavian blocking, while other circulation patterns do
23 not yield temperature trends during extremes.

1. Introduction

24 In western Europe, recent hot summers were characterized by highly anomalous meteo-
25 rological conditions. In these situations, such as 2003, the heat was prolonged and intense,
26 and the consequences were disastrous for society and ecosystems [*Schär and Jendritzky,*
27 2004; *Robine et al., 2008; Wreford and Adger, 2010; Poumadere et al., 2005; Ciais et al.,*
28 2005].

29 European surface temperature variations are influenced by processes that combine ra-
30 diative forcing, the large-scale atmospheric circulation and local phenomena. Over the last
31 five decades, most of the intense European heat events have been connected to prolonged
32 spells of anticyclonic circulation (Scandinavian blocking) and dry spring conditions in
33 Southern Europe [*Schär et al., 1999; Fischer et al., 2007; Mueller and Seneviratne, 2012;*
34 *Zampieri et al., 2009; Quesada et al., 2012; Vautard et al., 2007*]. However, the Summer
35 2011 was cool and preceded by a dry spring; the Summer 2013 was warm and preceded by
36 a wet spring; and the Summer 2015 was warm with persisting southerly atmospheric flows
37 and no lasting blocking episodes. In order to assess the robustness of the link between
38 heat events and atmospheric circulation, we perform a statistical and dynamical analysis
39 on a longer period (1871-2015).

40 Since anticyclones extend to a radius of few hundreds kilometers, such a connection
41 must be researched on a regional scale [*Della-Marta et al., 2007; Stefanon et al., 2012*].
42 Hence, we restrict our analysis to Western Europe in the region covering France and the
43 Iberian Peninsula, whose weather conditions are strongly influenced by the atmospheric
44 circulation over the North Atlantic.

2. Data and Methods

We base our analysis on the sea-level pressure (SLP) and the surface temperature fields during summers (June-July-August: JJA) in 20th Century Reanalysis data (20CR: 1871–2011, *Compo et al.* [2011]). To ensure the robustness of the results, we used the ensemble mean (EM) and 10 members (M0-M9) of the ensemble. The analysis is completed with other reanalysis products: NCEP (1948-2015) [*Kalnay et al.*, 1996] and ERA20C reanalysis (1900-2000) [*Poli et al.*, 2013] (see supplementary material). In order to describe the variability of the atmospheric circulation, we decompose the summer SLP field into weather regimes following the approach of *Yiou et al.* [2008] and study their connection with hot episodes at seasonal and sub-seasonal timescales.

2.1. Weather Regimes

Weather regimes are recurring states of the atmospheric circulation and provide a useful description of the atmospheric variability [*Michelangeli et al.*, 1995; *Corti et al.*, 1999]. Following the methods of *Michelangeli et al.* [1995] and *Yiou et al.* [2008] we compute four weather regimes ($k = 4$) over the North Atlantic region [$80^{\circ}\text{W} - 50^{\circ}\text{E}$; $20 - 70^{\circ}\text{N}$] (Fig. 1a-d) using the first ten Empirical Orthogonal Functions (EOFs) calculated on daily NCEP SLP data (reference period: 1970–2010) over the summers (JJA). The k-means algorithm is applied to the ten first EOFs of the SLP data to compute the four clusters. The Principal Components centroids are recomposed with the EOFs to obtain the weather regimes in physical space. To weigh the variations of the grid cell surface in the data we use the square root of cosine of latitude. For comparison, we reproduce NCEP weather regimes over different reanalysis datasets. All the reanalyses data we use

65 are interpolated on the same grid ($2.5^\circ \times 2.5^\circ$). The SLP data of all the reanalyses are
 66 projected by minimizing a Euclidean distance onto the NCEP weather regime centroids
 67 (in physical space). So, there is no further truncation of SLP data. Then, the SLP from all
 68 the datasets are classified according those four summer weather regimes (Fig. 1a-d) with
 69 the same nomenclature as *Cassou et al.* [2005]: a) the negative phase of North Atlantic
 70 Oscillation (NAO $-$) showing a dipole between Greenland and Northern Europe, b) the
 71 Atlantic Ridge (AR), with a high pressure over the center of the North Atlantic and some
 72 common features with the positive phase of NAO, c) Scandinavian Blocking (BLO), with
 73 a high pressure center over Scandinavia, d) Atlantic Low (AL), with a low pressure center
 74 covering the central North Atlantic.

75

2.2. Projection onto weather regimes for a dynamical representation

76 In order to visualize the dependence between the daily SLP fields and the four weather
 77 regimes, we represent the *trajectory* of each summer in the space of correlations (Fig.
 78 2a-c) using an approach based on dynamical systems theory [*Katok and Hasselblatt, 1997*]
 79 . In this framework, the motion of a particle is represented in the space defined by its
 80 position and speed (the so-called phase space). In our set-up, the particle is replaced by
 81 a SLP field and the directions in phase space correspond to the projections on the four
 82 weather regimes. Trajectories provide additional information with respect to the monthly
 83 average statistical quantities, on the time dependence and the coherence of the dynamical
 84 projection with respect to weather regime bases. If a trajectory jumps every day to a
 85 different region of the phase space, then a dominant weather regime is not representative

86 of the dynamical behavior of events lasting several days. If instead the trajectory occupies
87 a restricted region of the phase space with smooth transitions of the projection among
88 weather regimes, then the dynamical representation is informative and the basis of weather
89 regimes is appropriate. This is equivalent to assuming the existence of a low-dimensional
90 attractor. The caveat is that the weather regime description is a first order simplification
91 of the atmospheric circulation that captures large scale features. Although this phase-
92 space method has been debated since *Lorenz* [1991], there are theoretical [*Chekroun et al.*,
93 2011] and experimental evidences [*Casdagli et al.*, 1991] that such a procedure is effective
94 when the dynamics can be projected on a low dimensional phase space with a stochastic
95 perturbation.

3. Results

96 The link between atmospheric circulation and heat events is investigated at two
97 timescales: i) Seasonal: summers with high mean temperature anomalies, and ii) Subsea-
98 sonal: heatwaves defined as periods with high temperatures for at least five consecutive
99 days.

3.1. European weather regimes during the warmest summers

100 We carried out a statistical analysis of the 20 hottest summers of the period 1871–2011
101 (Fig. 1i). In Western-Europe [$10^{\circ}\text{W} - 7.5^{\circ}\text{E}$; $35 - 50^{\circ}\text{N}$], the 20 hottest summers (Fig.
102 1i and 2) are defined in each dataset as the ones having the highest average temperature
103 anomalies with respect to the climatology. Figure 1e-h show the anomalous summer fre-
104 quency of weather regimes in 20CR with respect to the NCEP reference period. In this
105 figure we see how NAO- is the unique regime decreasing in frequency with the time, and

106 BLO is the one increasing in frequency with the time. Figure 1i shows the dominant
107 regime as the one with the highest anomalous frequency. We find a general agreement
108 between all the 20CR members and the EM in terms of warmest summers and the dom-
109 inating weather regime. Most of the warmest summers (largest circles in Fig. 1e) occur
110 during the second part of the 20th century. As observed by *Stott et al.* [2004] and *Meehl*
111 *and Tebaldi* [2004], they also increase in frequency over time. Our analysis shows signif-
112 icant changes in the dominating weather regimes associated with warmest summers. If
113 BLO is dominant from the second part of 20th century, scarce occurrences of this weather
114 regime are found before 1930, even within the ensemble members of 20CR. BLO and AL
115 regimes are conducive to warm extremes and NAO- and AR are the opposite (Cassou et
116 al. 2005). Figure 1i shows that, after 1930, it is more frequent to find hottest summers
117 linked to what we know as warm regimes. BLO (the most frequent one after 1930) leads
118 to stagnant air and potential land-surface feedbacks, whereas AL relies on advection from
119 lower latitudes. In the other hand, NAO- is the dominant weather regime during warmer
120 summers up to 1930. This weather regime transports warm air from North Africa and
121 the Mediterranean into Europe. AR regime is more stable in time (Figure 1f, 1i).

122
123 To understand such trends we decompose the average information found with the sta-
124 tistical analysis via the dynamical representation of the warmest summers, defined in
125 section 2.2. We project the SLP anomaly fields onto NAO- and AR regimes, which are
126 the most frequent for the first part of the 20th century as shown in Fig. 1 e. This analysis
127 synthesizes the trajectory of the atmospheric circulation during heat events in a space

128 represented by the weather regimes. Consistently with the previous analysis, we find that
129 the atmospheric dynamics has evolved from patterns that are positively correlated with
130 NAO– during the second half of 19th century (Fig. 2 a), to negative correlations with
131 the pattern at the beginning of 21st century (Fig. 2 c), with a neutral state with respect
132 to the NAO in the middle of the 20th century (Fig. 2b). Similar projections on BLO
133 and AL regimes show: that BLO has the opposite change of NAO-, being positive during
134 the first period (Figure S4a) and negative during the last one (Figure S4c). AR and AL
135 regimes do not show significant differences between the periods. Those correlations add
136 a daily temporal information that is not captured by the analysis of the dominating sea-
137 sonal weather regime (Figure 1i) and highlight a change of atmospheric behavior. Thus
138 the dominant weather regimes are a valid concept as the trajectory of heatwaves persist
139 several days around the same region of the phase space. These changes are consistent
140 within the 20CR ensemble, as the M0-M9 average (Fig. 2d) shows consistent results with
141 the EM.

3.2. European weather regimes during heatwaves events

142 To understand whether those results hold also at sub-seasonal timescales (independently
143 from the fact that they have been observed during hot summers), we compute the average
144 temperature during heatwaves striking Western-Europe.

145 Heatwave events are defined when the summer temperature exceeds a threshold /per-
146 centiles (P90, P95) for more than 5 consecutive days. Figure 3 shows heatwave events
147 above the P90 threshold. Temperatures are de-trended by removing a linear trend calcu-
148 lated from the time series of summer seasonal means for each dataset. Heatwaves events

are grouped by the dominating weather regime. We find that 19% of total events are dominated by NAO– (Fig. 3a), 36%, by BLO (Fig. 3c). Heatwaves that are associated by AR (Fig. 3b) and AL (Fig. 3d) weather regimes have a frequency of 19% and 26%, respectively. Summer heatwave events dominated by BLO regime have an increasing trend of $0.12^{\circ}\text{C}/\text{decade}$ along the period reaching temperatures up to 29°C in the beginning of the 21st century. We also find that the longest events are associated to BLO regime (Fig. 3e). On the contrary, NAO– have a decreasing trend of $-0.06^{\circ}\text{C}/\text{decade}$ reaching 26°C at the end of the 19th century, and 24°C in the beginning of the 21st century. BLO is the only one with a significant trend.

To shed more light on the circulaion changes, we compute composites of SLP and surface temperature anomalies for pre-1930 heatwaves (figure 4a) and post-1930 heatwaves (4c) during all the heatwave events found in analysis of figure 3. The exercise is repeated by taking into account the occurrence of NAO– heatwave events for pre-1930 (4b) and the occurrence of BLO heatwave events for post-1930 (4d). The temperature pattern changes in pre and post 1930 maps mainly in Greenland and the East coast of North America and in Europe. Pressure patterns for all the heatwave events pre and post-1930 reproduce well NAO– and BLO (respectively) albeit weaker for the BLO regime. So, even if there is a change for NAO–, BLO is the one with a stronger change for short-term events, because it is the most representative pattern in heatwaves events from 1930.

4. Discussion and conclusions

These results confirm that most heat events (either warmest summers and heatwaves in Western Europe) of the second half of the 20th century occurred when the Scandina-

170 vian Blocking weather regime dominated the North Atlantic region, causing increasing
171 temperatures and more frequent and longer heatwaves events (figure 3 and figure S7).
172 Our results also show that, before 1930, NAO– is more favorable to drive heatwaves
173 events and warm summers. Although the increasing temperature trends observed during
174 blocking heatwaves episodes could be attributed to the climate change, the change in the
175 dominating weather regimes may have a different explanation, e.g. the decadal variability
176 of the atmospheric dynamics.

177 The robustness of our results is ensured by the use of 20CR ensemble and other reanal-
178 ysis datasets (see supplementary material).

179 The dynamical analysis also suggests that there is an increase of negative correlations
180 between warmest summers and the NAO– regime. The consequence of those trends (in
181 temperature and BLO circulation) is an increased risk of summer heatwaves like 2003,
182 with the associated impacts on ozone pollution because blocking episodes yield reduced
183 wind over Europe [*Solberg et al.*, 2008].

184
185 Although the information extracted in warmest summers and heatwaves is a priori
186 different, our analysis shows similar results at different timescales: NAO– was the most
187 representative pattern in warmer summers and heatwaves events up to 1930 and from
188 1930 on, BLO is the most representative one, with exceptions in some specific cases (e.g.
189 Summer 2003 is dominated by AL regime but the heatwave episodes are dominated by
190 AL and BLO regimes; BLO is associated to the longest and hottest heatwave). In the
191 debate on the mechanisms leading to changes in the atmospheric circulation [*Shepherd*,

192 2014], our results demonstrate the signature of the impacts of the atmospheric circulation
193 on European heat events.

194 **Acknowledgments.** M.C.A-C. was supported by MILEX project, funded by *Swedish*
195 *Research Council*, grant number C0629701. D.F. and P.Y. were supported by A2C2
196 project, funded by the *ERC*, grant number 338965. The authors are thankful to G.
197 Compo, for the help supported with data from members of 20CR reanalysis. 20CR and
198 NCEP Reanalysis data provided by the NOAA/OAR/ESRL PSD, Boulder, Colorado,
199 USA, from their Web site at <http://www.esrl.noaa.gov/psd/>. ERA-20C reanalysis data
200 provided by the ECMWF (European Centre for Medium-Range Weather Forecasts), Read-
201 ing, UK, from their website at <http://apps.ecmwf.int/datasets/data/era20c-daily/>.

202
203 **Author contributions:** M.C.A-C. carried out the computation of warmer summers
204 and Heatwave events and their relation with weather regimes. D.F. analyzed that relation
205 from the dynamical systems point of view. P.Y. advised the work and carried out the
206 weather regime analysis. All authors contributed to the writing and correcting of the
207 manuscript and with the design of the work.

208
209 **Supplementary information** is available in the online version of the paper. Cor-
210 respondence and requests for materials should be addressed to M.C.A-C (email:
211 carmen.alvarez-castro@lsce.ipsl.fr).

References

- 212 Casdagli, M., S. Eubank, J. D. Farmer, and J. Gibson (1991), State space reconstruction
213 in the presence of noise, *Physica D.*, *51*(1), 52–98.
- 214 Cassou, C., L. Terray, and A. S. Phillips (2005), Tropical atlantic influence on European
215 heat waves, *J. Climate*, *18*(15), 2805–2811.
- 216 Chekroun, M. D., E. Simonnet, and M. Ghil (2011), Stochastic climate dynamics: Random
217 attractors and time-dependent invariant measures, *Physica D.*, *240*(21), 1685–1700.
- 218 Ciais, P., et al. (2005), Europe-wide reduction in primary productivity caused by the heat
219 and drought in 2003, *Nature*, *437*(7058), 529–533.
- 220 Compo, G. P., et al. (2011), The twentieth century reanalysis project, *Q. J. Roy. Meteor.*
221 *Soc.*, *137*(654), 1–28.
- 222 Corti, S., F. Molteni, and T. Palmer (1999), Signature of recent climate change in fre-
223 quencies of natural atmospheric circulation regimes, *Nature*, *398*(6730), 799–802.
- 224 Della-Marta, P. M., J. Luterbacher, H. von Weissenfluh, E. Xoplaki, M. Brunet, and
225 H. Wanner (2007), Summer heat waves over western Europe 1880–2003, their relation-
226 ship to large-scale forcings and predictability, *Clim. Dynam.*, *29*(2-3), 251–275.
- 227 Fischer, E., S. Seneviratne, D. Lüthi, and C. Schär (2007), Contribution of land-
228 atmosphere coupling to recent European summer heat waves, *Geophys. Res. Lett.*, *34*(6),
229 doi:10.1029/2006GL029068.
- 230 Kalnay, E., et al. (1996), The NCEP/NCAR 40-year reanalysis project, *B. AM. Meteorol.*
231 *Soc.*, *77*(3), 437–471.

- 232 Katok, A., and B. Hasselblatt (1997), *Introduction to the modern theory of dynamical*
233 *systems*, vol. 54, Cambridge University Press.
- 234 Lorenz, E. N. (1991), Dimension of weather and climate attractors, *Nature*, 353(6341),
235 241–244.
- 236 Meehl, G. A., and C. Tebaldi (2004), More intense, more frequent, and longer lasting heat
237 waves in the 21st century, *Science*, 305(5686), 994–997.
- 238 Michelangeli, P.-A., R. Vautard, and B. Legras (1995), Weather regimes: Recurrence and
239 quasi stationarity, *J. Atmos. Sci.*, 52(8), 1237–1256.
- 240 Mueller, B., and S. I. Seneviratne (2012), Hot days induced by precipitation deficits at
241 the global scale, *Proc. Natl. Acad. Sci.*, 109(31), 12,398–12,403.
- 242 Poli, P., et al. (2013), The data assimilation system and initial performance evaluation
243 of the ecmwf pilot reanalysis of the 20th-century assimilating surface observations only
244 (ERA-20C), *ECMWF ERA Rep*, 14, 59.
- 245 Poumadere, M., C. Mays, S. Le Mer, and R. Blong (2005), The 2003 heat wave in France:
246 dangerous climate change here and now, *Risk Anal.*, 25(6), 1483–1494.
- 247 Quesada, B., R. Vautard, P. Yiou, M. Hirschi, and S. I. Seneviratne (2012), Asymmetric
248 European summer heat predictability from wet and dry southern winters and springs,
249 *Nature Clim. Change*, 2(10), 736–741.
- 250 Robine, J.-M., S. L. K. Cheung, S. Le Roy, H. Van Oyen, C. Griffiths, J.-P. Michel, and
251 F. R. Herrmann (2008), Death toll exceeded 70,000 in Europe during the summer of
252 2003, *C. R. Biol.*, 331(2), 171–178.

- 253 Schär, C., and G. Jendritzky (2004), Climate change: hot news from summer 2003, *Nature*,
254 *432*(7017), 559–560.
- 255 Schär, C., D. Lüthi, U. Beyerle, and E. Heise (1999), The soil-precipitation feedback: A
256 process study with a regional climate model, *J. Climate*, *12*(3), 722–741.
- 257 Shepherd, T. G. (2014), Atmospheric circulation as a source of uncertainty in climate
258 change projections, *Nat. Geosci.*, *7*(703-708).
- 259 Solberg, S., Ø. Hov, A. Søvde, I. Isaksen, P. Coddeville, H. De Backer, C. Forster, Y. Or-
260 solini, and K. Uhse (2008), European surface ozone in the extreme summer 2003, *J.*
261 *Geophys. Res.*, *113*(D7).
- 262 Stefanon, M., F. D’Andrea, and P. Drobinski (2012), Heatwave classification over Europe
263 and the Mediterranean region, *Environ. Res. Lett.*, *7*(1), 014,023.
- 264 Stott, P. A., D. A. Stone, and M. R. Allen (2004), Human contribution to the European
265 heatwave of 2003, *Nature*, *432*(7017), 610–614.
- 266 Vautard, R., P. Yiou, F. D’andrea, N. De Noblet, N. Viovy, C. Cassou, J. Polcher, P. Ciais,
267 M. Kageyama, and Y. Fan (2007), Summertime European heat and drought waves
268 induced by wintertime Mediterranean rainfall deficit, *Geophys. Res. Lett.*, *34*(7), doi:
269 10.1029/2006GL028001.
- 270 Wreford, A., and W. N. Adger (2010), Adaptation in agriculture: historic effects of heat
271 waves and droughts on UK agriculture, *Int. J. Agric. Sustain.*, *8*(4), 278–289.
- 272 Yiou, P., et al. (2008), Weather regime dependence of extreme value statistics for sum-
273 mer temperature and precipitation, *Nonlinear Proc. Geoph.*, *15*(3), 365–378, doi:
274 10.5194/npg-15-365-2008.

275 Zampieri, M., F. D'Andrea, R. Vautard, P. Ciais, N. de Noblet-Ducoudré, and P. Yiou
276 (2009), Hot European summers and the role of soil moisture in the propagation of
277 mediterranean drought, *J. Climate*, 22(18), 4747–4758.

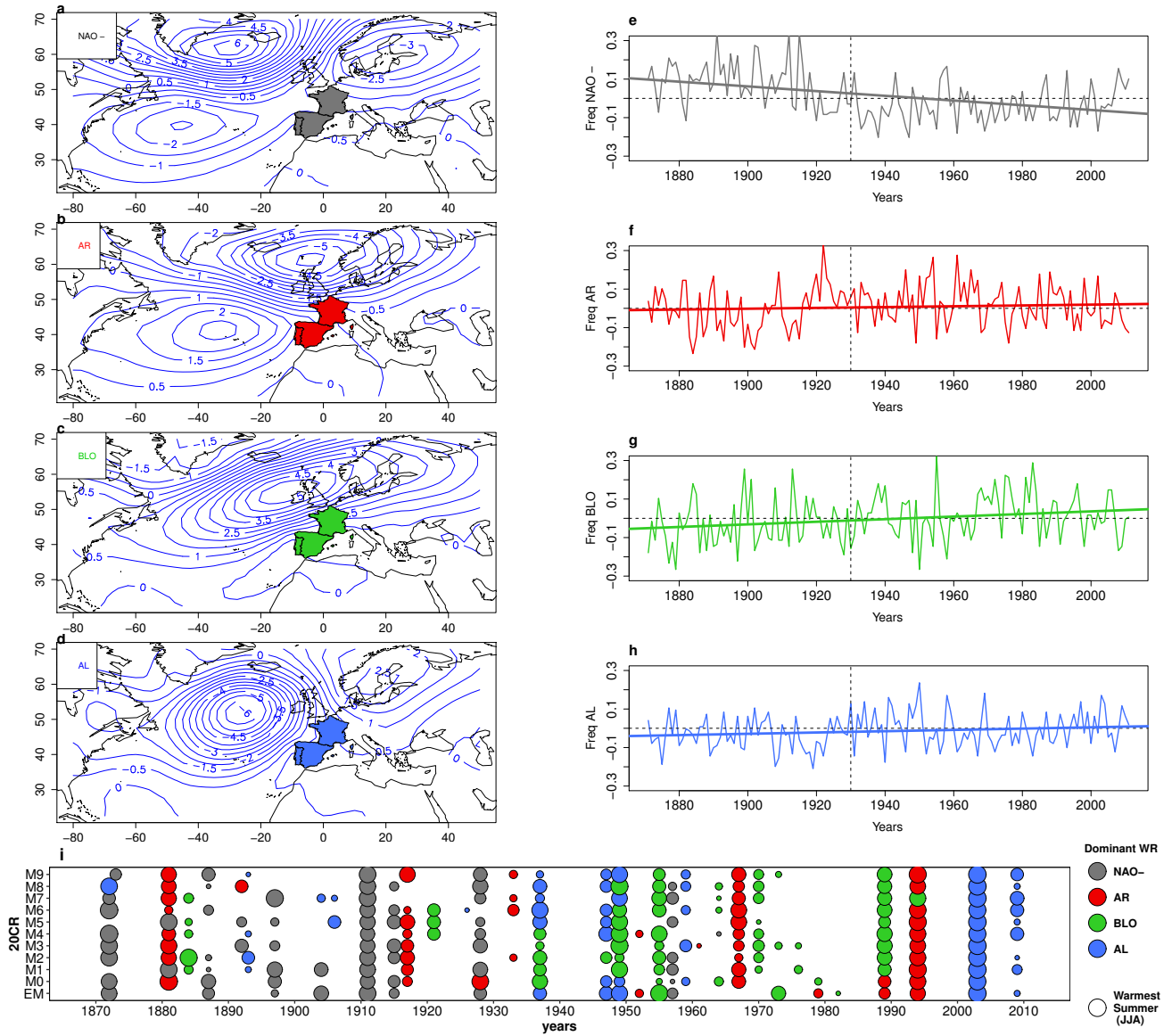


Figure 1. Summer SLP weather regimes over the North-Atlantic region and their dominance in the twenty warmest summers during 1871-2011 in Western-Europe. **a-d**, Summer SLP (hPa anomalies) Weather regimes: **a**, North Atlantic Oscillation in its negative phase (NAO-). **b**, Atlantic Ridge (AR). **c**, Blocking (BLO). **d**, Atlantic Low (AL) weather regime. **e-h**, Long-term weather regime frequency (anomalies) with respect the reference period (NCEP 1970-2010) **i**, Twenty warmest summers in Western-Europe (colored region in **a-d**) with their dominant weather regime. Years are shown in *x* axis, while *y* axis displays each of the 20CR members (M0 – M9) and the 20CR EM. Circle size depends on temperature (anomalies), the largest the warmest. Colors represents the dominant weather regime for each summer based in the highest anomalous frequency in **e-h**.

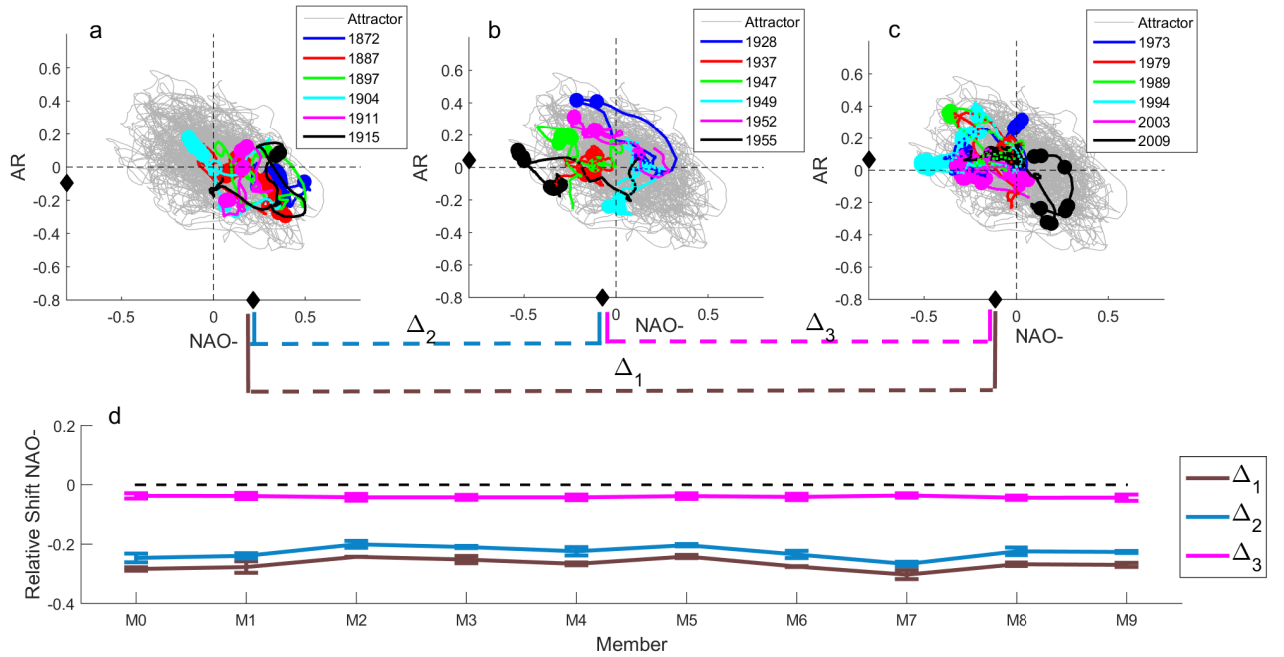


Figure 2. Dynamical representation of the warmest summers. **a-c**, Correlations of daily SLP fields and NAO- (x -axis), AR (y -axis) weather regimes for three different periods. Warmest summers are colored as in the legend, light grey lines represent all data. Big circles represent days with temperature above 85th percentile. Average correlations of warmest summers with respect to the NAO- weather regimes (black circle on x -axis) and relative difference between the periods ($\Delta_1 - 2 - 3$) for each member of the ensemble (**d**). Errorbars correspond to the standard deviation of the mean. A moving average filter with a 30 day window has been applied to the data.

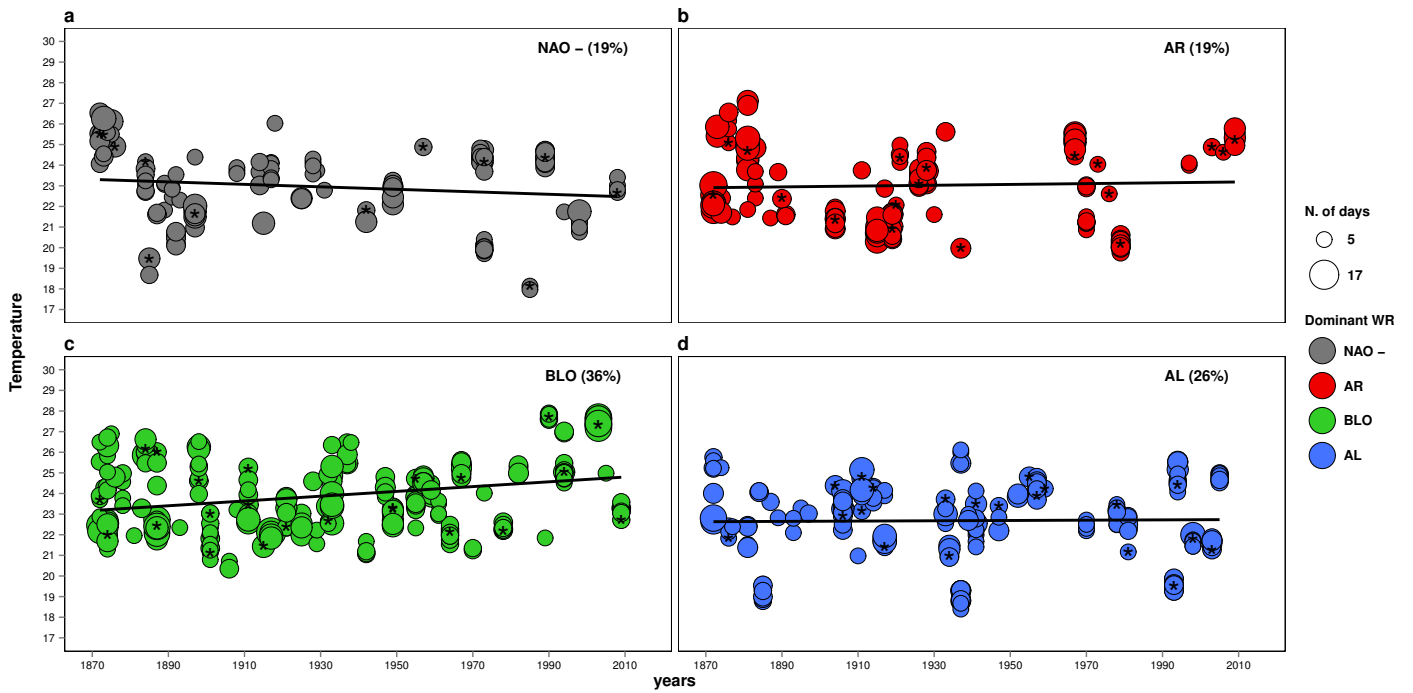


Figure 3. Dominant weather regimes during Summer heatwave events. In a–d, Summer heatwave events (90th Percentile) for members and EM (circles with stars) of 20CR data, 1871–2011. Colors correspond to the dominant weather regime in each event, temperature (y -axis) and years (x -axis). Circle sizes depend on the event duration by number of days, the larger the longer duration. Percentages show the frequency of each weather regime. Linear fits are shown in black solid lines. e, Temperature vs number of days for each heatwave event (circles). Solid lines show linear fits to data. Colors in solid lines and circles correspond to the weather regime. Dotted lines represent percentiles (25th, 50th, 90th).

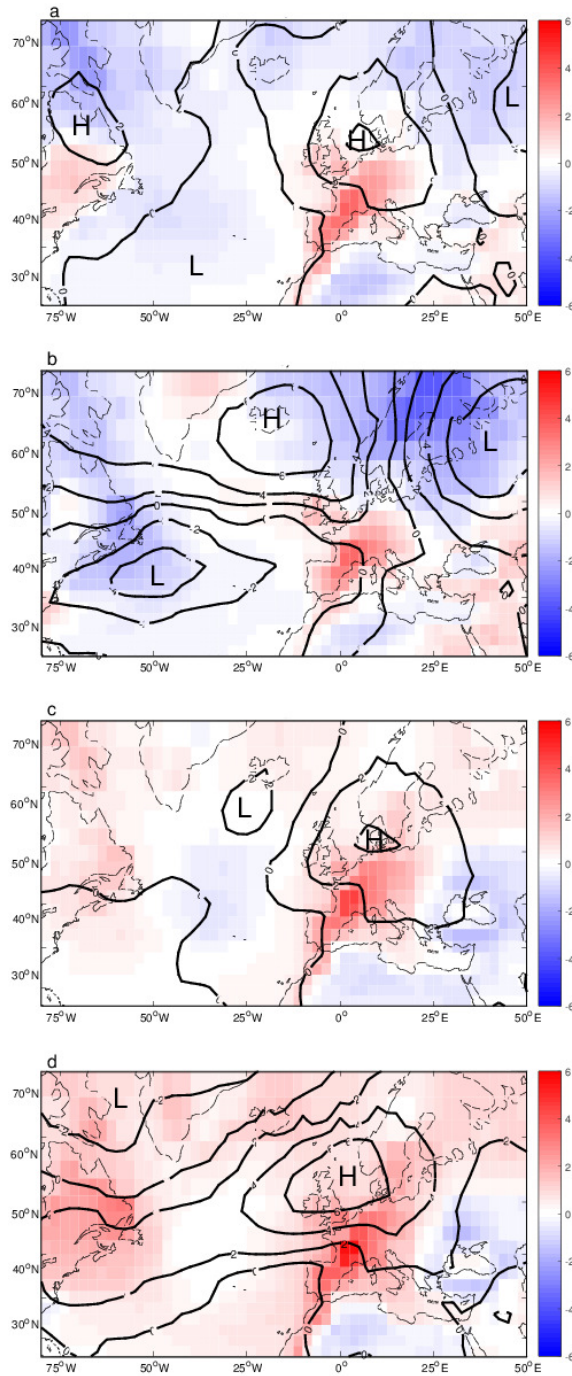


Figure 4. Composites of Sea Level Pressure (SLP) and Surface Temperature anomalies (SAT) pre/post 1930. In a–b, composites SLP and SAT for a) all the days during heatwaves events found before 1930, in b) just the events where NAO- was the dominant weather regime. In c–d, composites SLP and SAT for c) all days during heatwaves events found after 1930, in d) just the events where BLO was the dominant regime.

1 Changes in the atmospheric dynamics leading to
2 West European summer hot temperatures since 1900

M. Carmen Alvarez-Castro,¹ Davide Faranda,¹ and Pascal Yiou¹

Corresponding author: M. Carmen Alvarez-Castro, LSCE. (carmen.alvarez-castro@lsce.ipsl.fr)

¹Laboratoire des Sciences du Climat et de
l' Environnement, UMR 8212
CEA-CNRS-UVSQ, IPSL, Université
Paris-Saclay, F-91191 Gif-sur-Yvette, France

3 **Supplementary Material**

4 • Figure S1: Relative long-term summer weather regime frequency over the North-
5 Atlantic region and their dominance in warmest summers in Western-Europe (1871-2015)
6 using three reanalysis products (20CR, ERA20C, NCEP).

7 • Figure S2: Summer average temperatures for Western-Europe for three reanalysis
8 products (20CR, ERA20C, NCEP).

9 • Figure S3: Temperature anomalies during warmest summers (IP-France) with dom-
10 inance of each weather regime in three reanalysis products (20CR, ERA20C, NCEP).

11 • Figure S4: Dynamical representation of the warmest summers for 20CR Ensemble
12 mean during 1871-2011 in regimes BLO-AL.

13 • Figure S5: Dynamical representation of the warmest summers for ERA20C during
14 1900-2010 in regimes AR-NAO- and BLO-AL.

15 • Figure S6: Dominants weather regimes during Summer Heatwave events in Western-
16 Europe for three reanalysis products (20CR, ERA20C, NCEP).

17 • Figure S7: Temperature (y-axis) vs numbers of days (x-axis) during each heatwave
18 event for the 20CR Ensemble Mean (1871-2011) weather regimes.

19 • Table S1: Absolute root mean square error by period and weather regime.

20 • Table S2: p-values of Heatwaves events in each dataset.

Abs_{RMSE}	Period	NAO-	AR	BLO	AL
NCEP	(1970-2010)	1.01	1.00	0.98	0.99
	(1948-2015)	1.01	1.0	1.01	1.00
ERA 20C	(1900-1936)	0.95	0.99	0.96	0.97
	(1937-1973)	1.03	0.99	1.01	1.01
	(1974-2010)	1.03	1.01	1.03	1.03
20CR	(1871-1917)	0.94	1.01	1.00	0.99
	(1918-1964)	1.03	0.98	1.02	1.01
	(1965-2011)	1.04	1.01	0.99	1.01

Table S 1. Absolute error of the Root mean square deviation (Abs_{RMSE}) of the truncated EOFs during the training period(NCEP:1970-2010) by Weather Regimes during summer in Western-Europe (see also Figure S8)

p-value	NAO-	AR	BLO	AL
M0	0,42	0,56	0,20	0,23
M1	0,57	0,53	0,23	0,32
M2	0,67	0,82	0,07	0,80
M3	0,88	0,74	0,09	0,87
M4	0,65	0,94	0,13	0,79
M5	0,81	0,91	0,09	0,54
M6	0,29	0,84	0,27	1,00
M7	0,18	0,53	0,30	0,80
M8	0,38	0,47	0,05	0,57
M9	0,71	0,63	0,45	0,81
EM 20CR	0,40	0,44	0,23	0,25
ERA 20C	0,32	0,37	0,30	0,65
NCEP	0,26	0,00	0,50	0,24
Mean 20C	0,54	0,67	0,19	0,63
Mean rea.	0,33	0,27	0,34	0,38

Table S 2. p-values of Heatwave events calculate for each dataset and regime. Mean 20C is the mean of all the members with EM20CR (trend line in figure 3) and Mean rean. is the mean of all the reanalyses (EM20CR, ERA20C, NCEP) (trend line in figure S6).

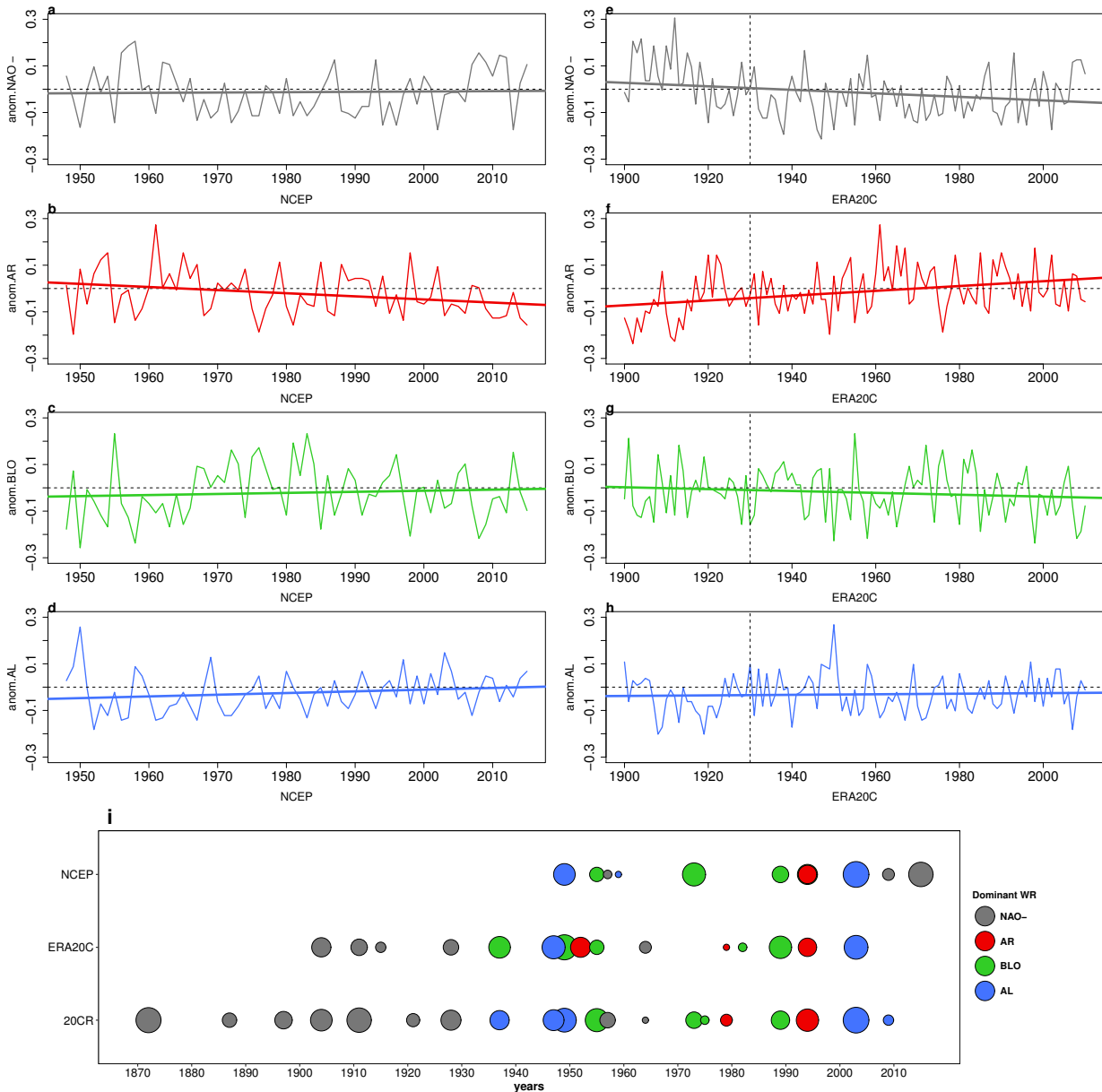


Figure S 1. Relative long-term summer weather regime frequency over the North-Atlantic region and their dominance in warmest summers in Western-Europe (1871-2015) using three reanalysis products (20CR, ERA20C, NCEP). As in figure 1, relative frequency of Summer SLP (hPa anomalies) weather regimes: NAO- (a,e), AR (b,f), BLO (c,g) and AL (d,h), but considering NCEP data (a-d,) and ERA20C (e-h). e, Warmest summers from 1871 to 2015 in Western-Europe with their dominant weather regime. Years are shown in x axis while y axis display each of the reanalysis products (20CR, ERA20C, NCEP). Circle size depends on temperature anomalies, the largest the warmest. Colors (black, red, green, blue) represents the dominant weather regime (NAO-, AR, BLO, AL) for each summer. The number of warmest summers are ponderate with the length of each dataset.

D R A F T September 20, 2016, 8:20pm D R A F T

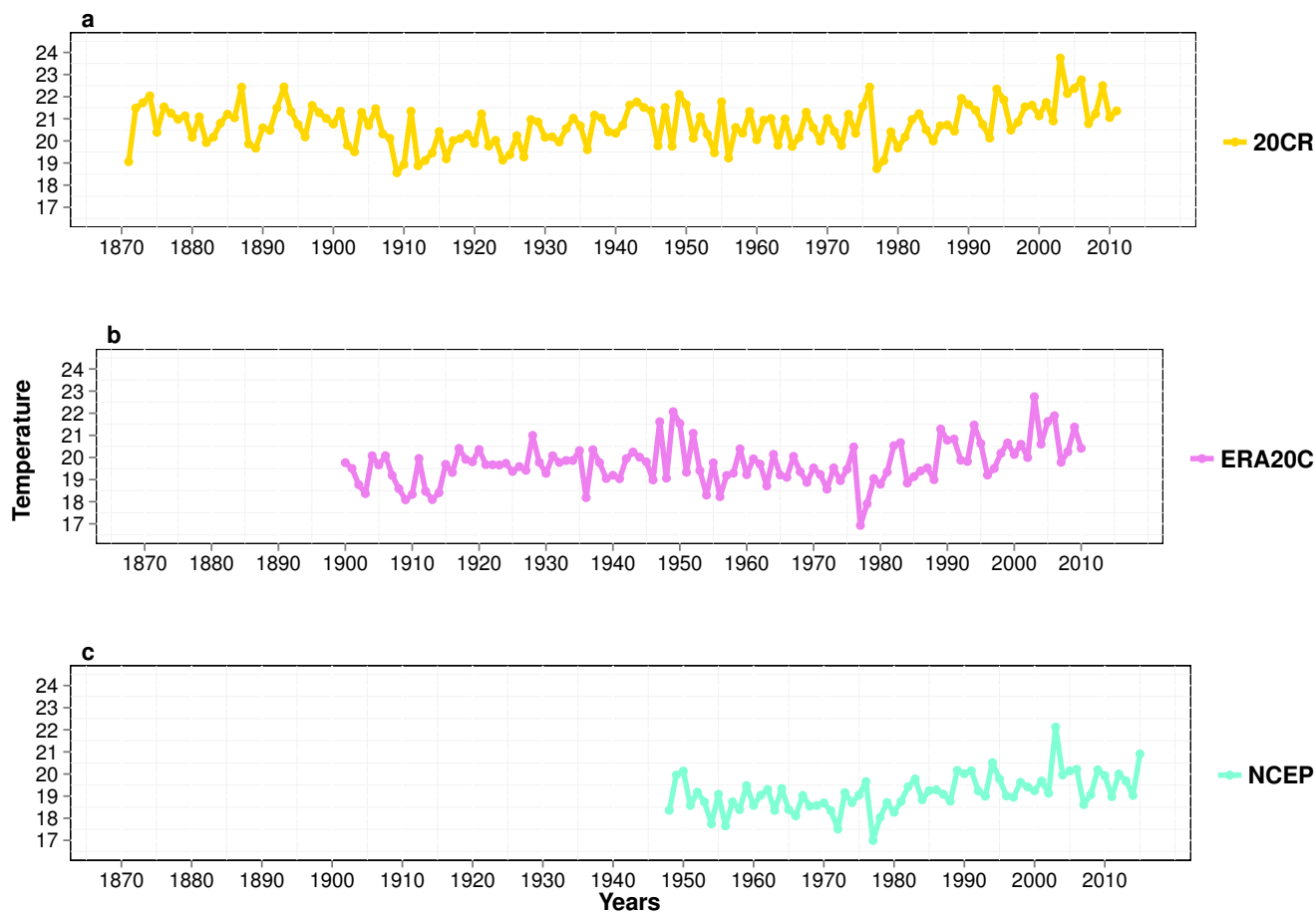


Figure S 2. Summer average temperatures ($^{\circ}\text{C}$) for Western-Europe. a, 20CR b, ERA20C and c, NCEP).

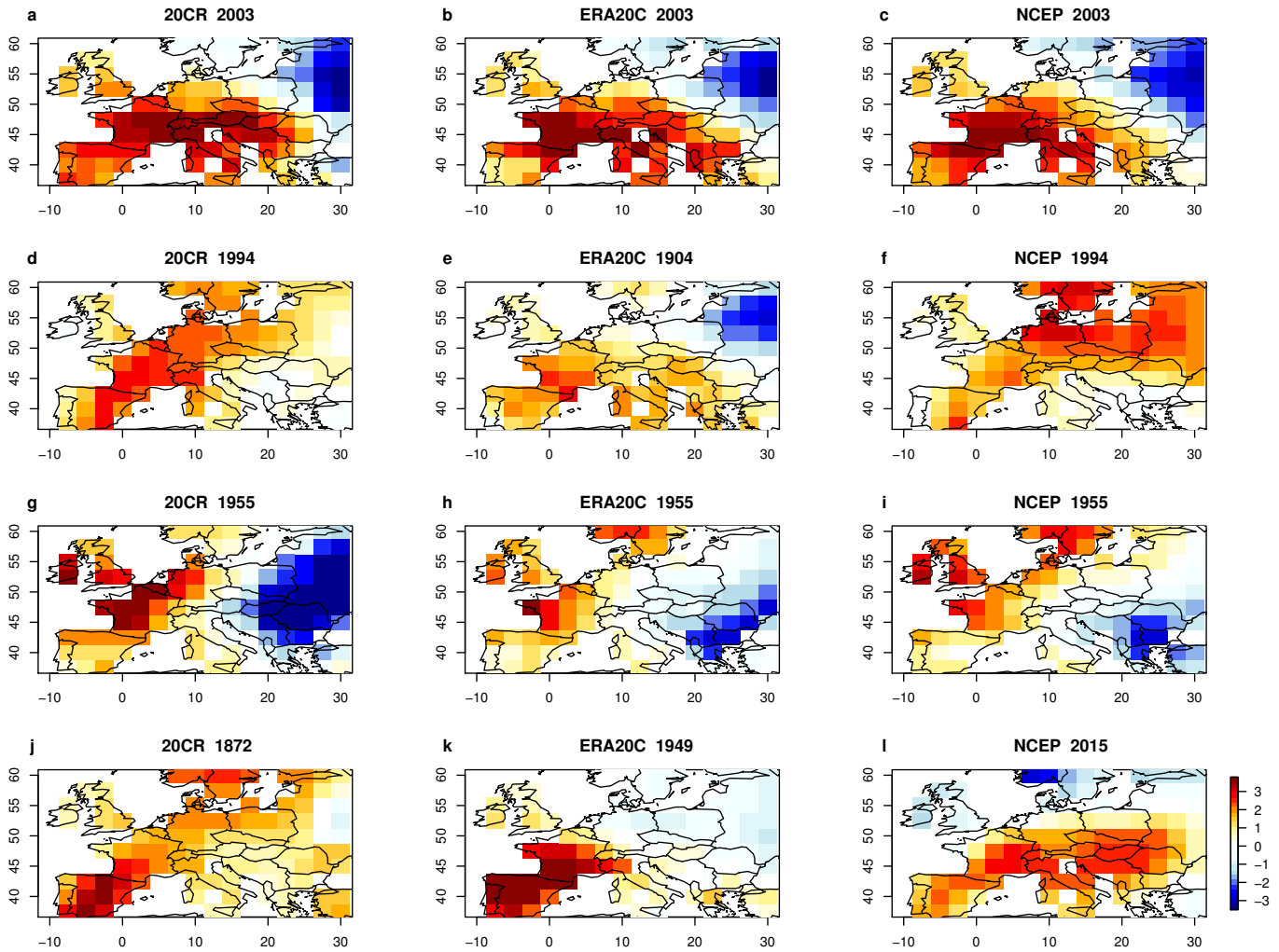


Figure S 3. Temperature anomalies maps for warmest summers in Western-Europe.

Each row correspond to a different dominant weather regime for some explanatory summers. Each column is a different reanalysis product. **a-c**, Summer 2003, where AL was the dominant weather regime. **d-f**, Summer of 1994, where AR was the dominant weather regime (Same frequencies of BLO and AR for NCEP during this summer). **g-i**, Summer of 1955, where BLO was the dominant weather regime. **j-l**, Since there is not a common summer for all the reanalysis datasets with NAO- as a dominant weather regime, here we show the most warmest summer (1872, 1904, 2015) where NAO- was the dominant weather regime in each reanalysis dataset (20CR, ERA20C, NCEP).

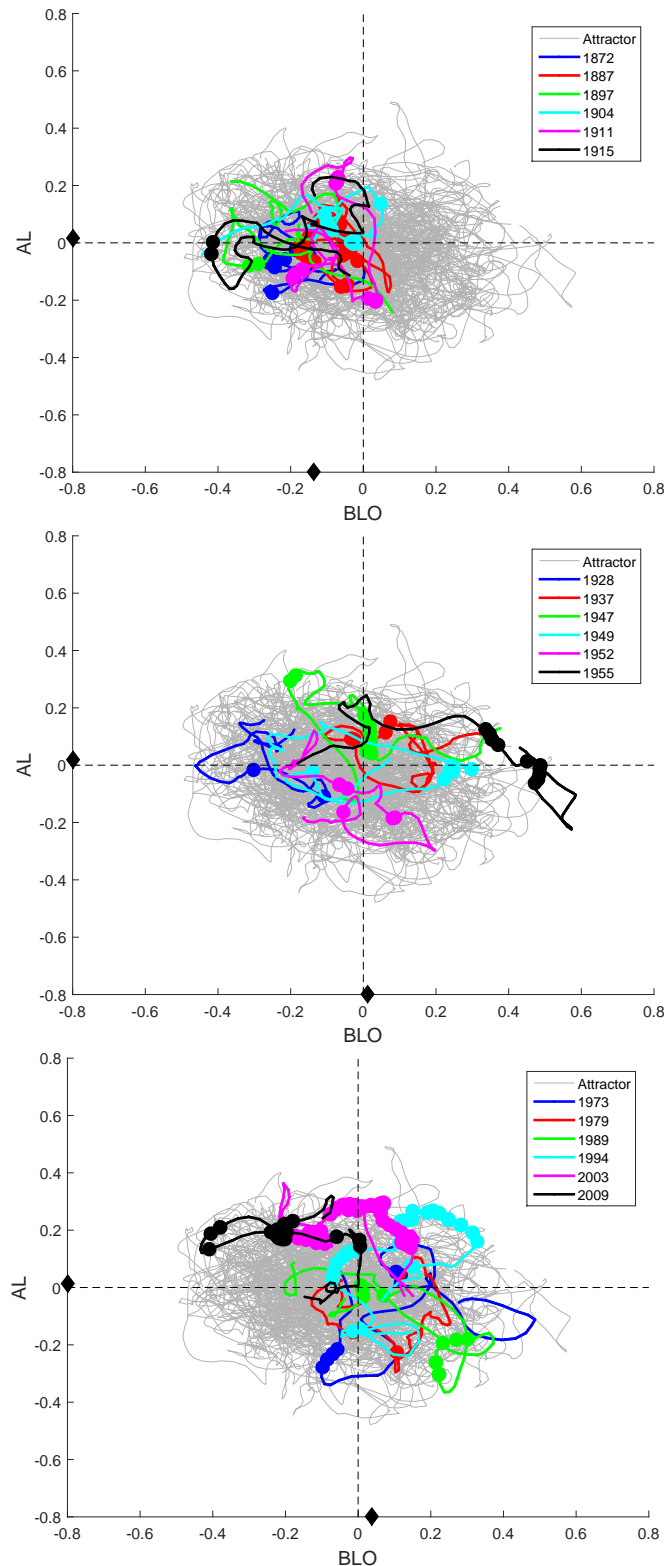


Figure S 4. Dynamical representation of the warmest summers (same method as fig.2a-c in main text) for 20CR during 1871-2011. Correlations of daily SLP fields and BLO (x-axis), AL (y-axis) weather regimes for three different periods. Warmest summers are colored as in the legend, light grey lines represent all data. Big circles represent days with temperature above the 85th percentile. Average correlations of warmest summers with respect to each weather regime (black circle on x-axis).

D R A F T

September 20, 2016, 8:20pm

D R A F T

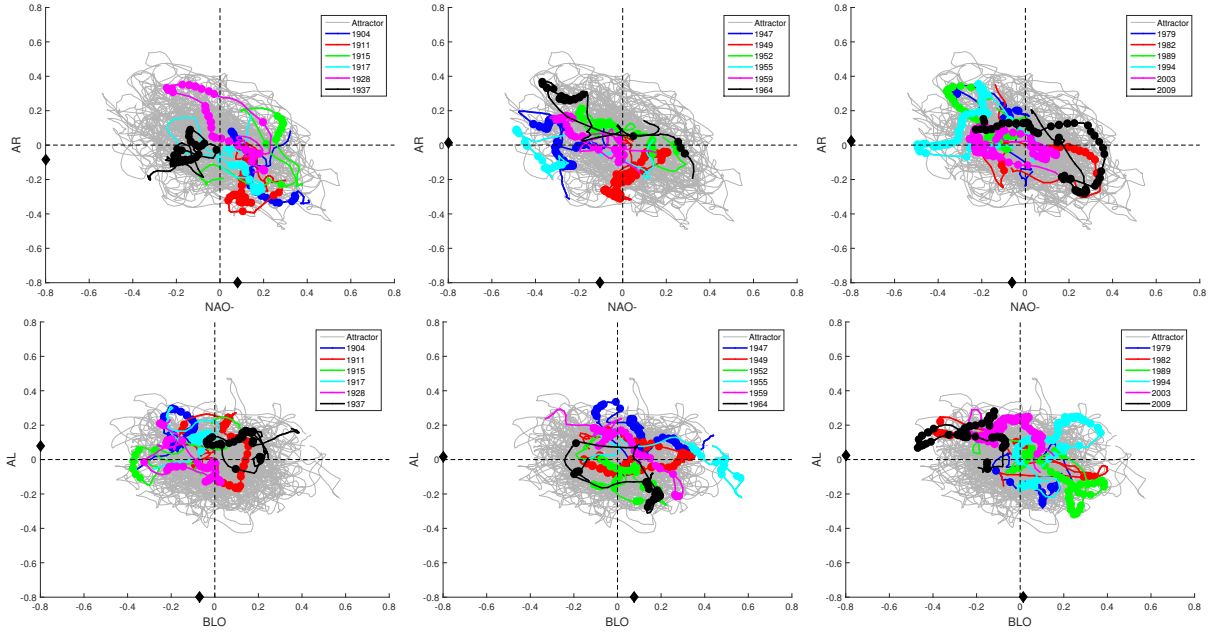


Figure S 5. Dynamical representation of the warmest summers (same as fig.2a-c in main text) for ERA20C during 1900-2010. Correlations of daily SLP fields and NAO- (x-axis), AR (y-axis) weather regimes in upper panels and correlations of daily SLP fields and BLO (x-axis), AL (y-axis) weather regimes in the bottom panels for three different periods. Warmest summers are colored as in the legend, light grey lines represent all data. Big circles represent days with temperature above 85th percentile. Average correlations of warmest summers with respect to each weather regime (black circle on x-axis).

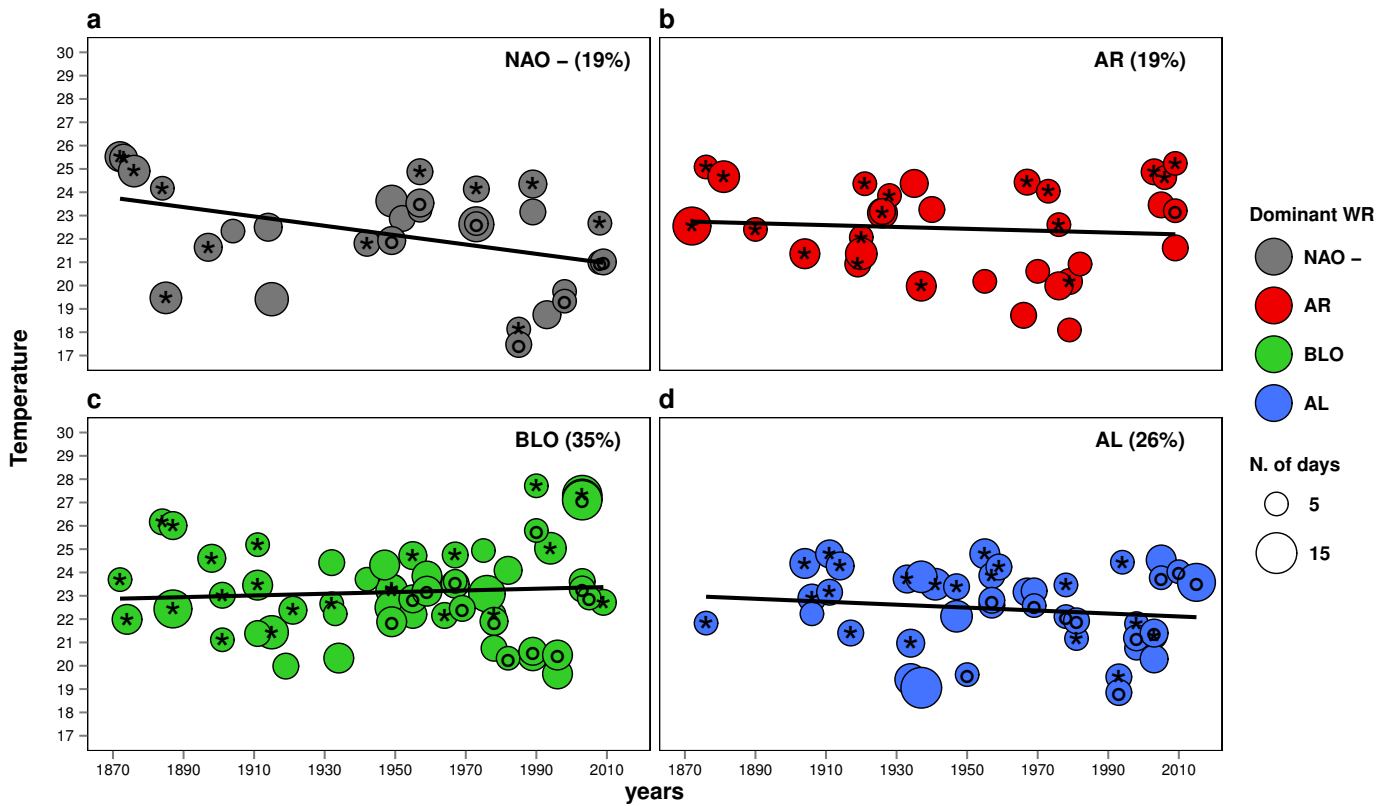


Figure S 6. Dominant weather regimes during Summer Heatwave events in Western-Europe. Summer heatwave events (P90th Percentile) from 1871 to 2015 for different reanalysis products: 20CR (circle with stars), ERA20C (empty circle), and NCEP (circles with inner circle). Colors correspond to the dominant Weather regime (a-d,) in each event, temperature (y-axis) and years (x-axis). Circle sizes depend on the event duration by number of days, the larger the longer duration. Percentages show the frequency of each weather regime. Linear fits are shown in black solid lines.

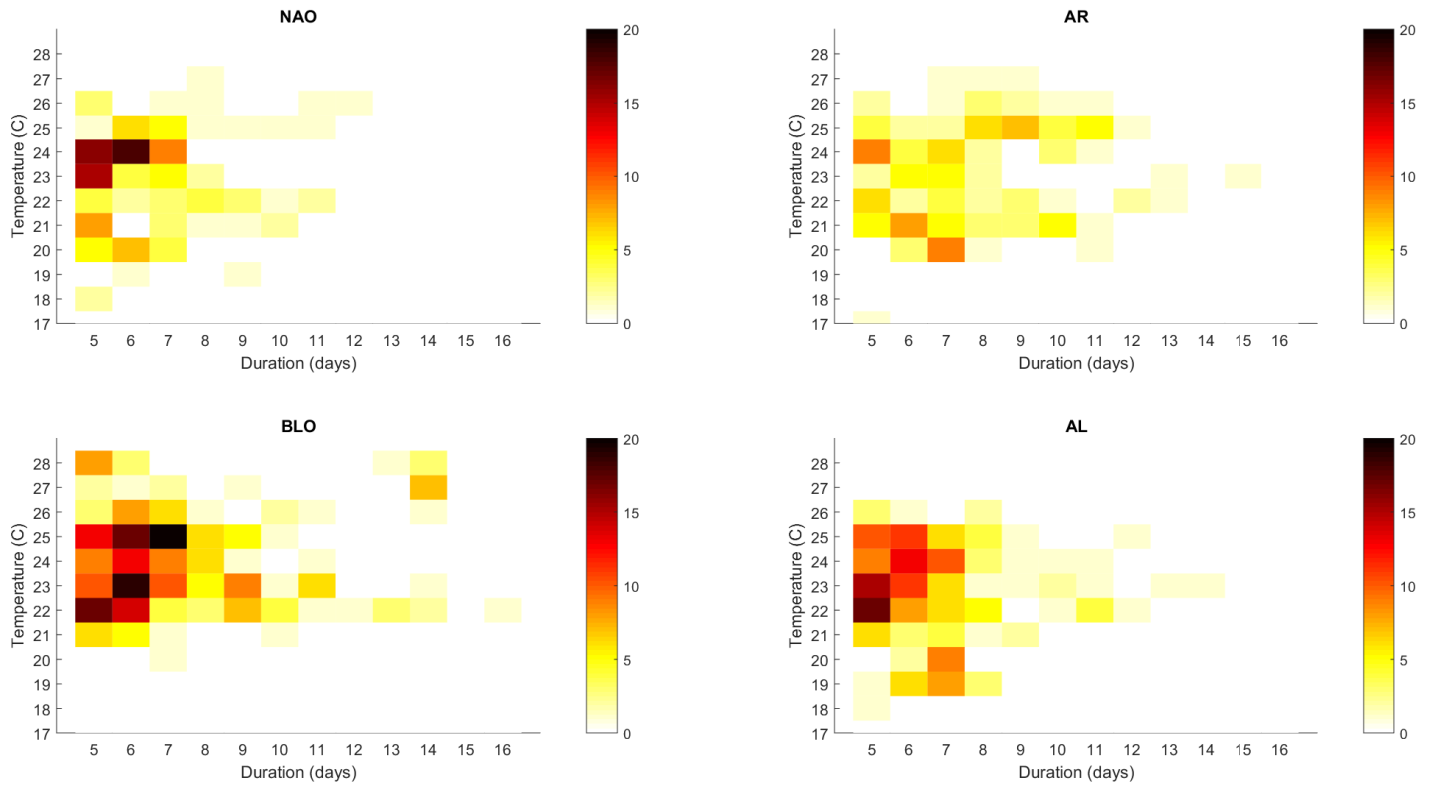


Figure S 7. Density plot of heatwave events. Temperature (y-axis) vs numbers of days (x-axis) during each heatwave event for the 20CR Ensemble Mean (1871-2011) weather regimes. Colors represent the number of heatwave events.

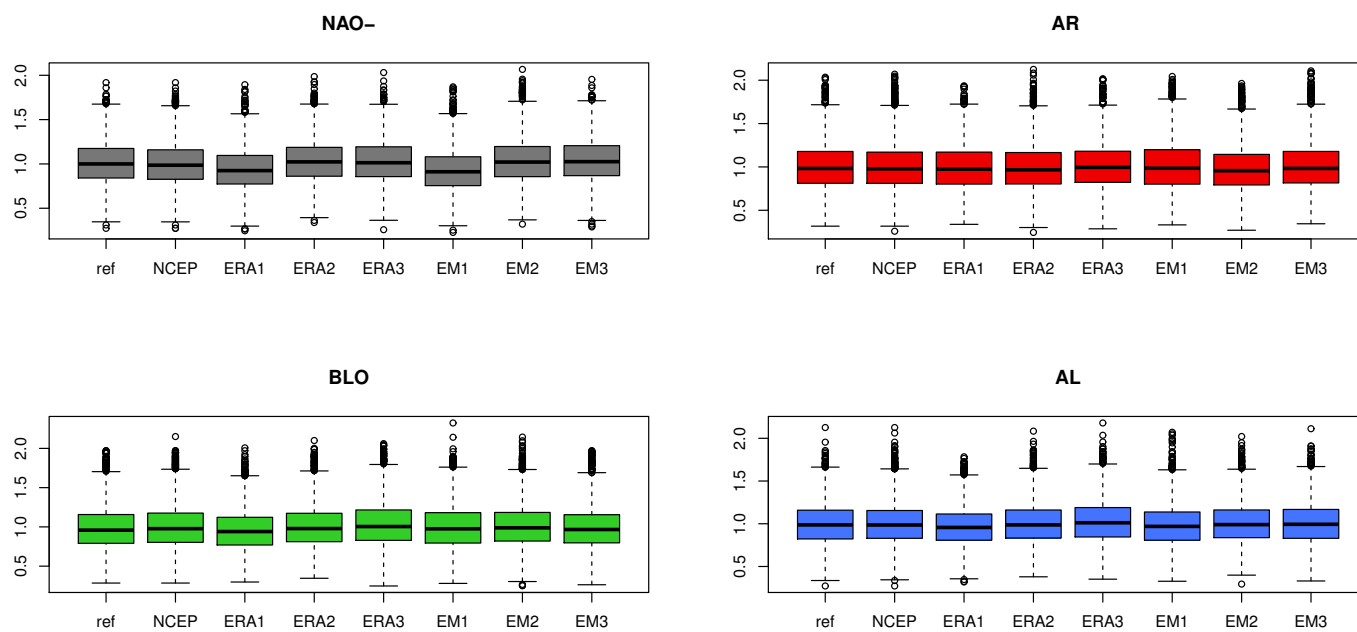


Figure S 8. Boxplots of Absolute Root Mean Square Error by period and weather regime. Colors represent each weather regime. (See also Table S1).